

The mapping of visual space by dragonfly lateral ocelli

Richard Berry · Joshua van Kleef ·
Gert Stange

Received: 14 November 2006 / Revised: 19 December 2006 / Accepted: 27 December 2006 / Published online: 2 February 2007
© Springer-Verlag 2007

Abstract We study the extent to which the lateral ocelli of dragonflies are able to resolve and map spatial information, following the recent finding that the median ocellus is adapted for spatial resolution around the horizon. Physiological optics are investigated by the hanging-drop technique and related to morphology as determined by sectioning and three-dimensional reconstruction. L-neuron morphology and physiology are investigated by intracellular electrophysiology, white noise analysis and iontophoretic dye injection. The lateral ocellar lens consists of a strongly curved outer surface, and two distinct inner surfaces that separate the retina into dorsal and ventral components. The focal plane lies within the dorsal retina but proximal to the ventral retina. Three identified L-neurons innervate the dorsal retina and extend the one-dimensional mapping arrangement of median ocellar L-neurons, with fields of view that are directed at the horizon. One further L-neuron innervates the ventral retina and is adapted for wide-field intensity summation. In both median and lateral ocelli, a distinct subclass of descending L-neuron carries multi-sensory information via graded and regenerative potentials. Dragonfly ocelli are adapted for high sensitivity as well

as a modicum of resolution, especially in elevation, suggesting a role for attitude stabilisation by localization of the horizon.

Keywords Dragonfly · Ocelli · Optics · L-neuron · Receptive field

Abbreviations

BFD	Back focal distance
LCD	Liquid crystal display
L-neuron	Large second-order ocellar neuron
LED	Light emitting diode
PSL	Posterior slope
S-neuron	Small second-order ocellar neuron
UV	Ultraviolet

Introduction

In their most common form, found for example in flies, bees, cicadas and damselflies, the dorsal ocelli of adult insects occur as a triplet that is located between the compound eyes on the apex of the head (reviewed in Goodman 1981). The median ocellus is principally directed forwards and upwards, while the lateral ocelli are directed sideways and upwards. The external appearance and size of the median ocellus is typically similar to those of the lateral ocelli.

Conversely, the ocelli of most recent families of anisopteran dragonflies are not located on the apex of the head, but are instead located frontally, just above the mandibles and below the holoptic compound eyes (Stange 1981). The median and lateral ocelli are quite

R. Berry · J. van Kleef · G. Stange
Centre for Visual Sciences,
Research School of Biological Sciences,
Australian National University, Canberra, Australia

R. Berry (✉)
Research School of Biological Sciences,
Australian National University,
PO Box 475, Canberra ACT 2601, Australia
e-mail: rberry@rsbs.anu.edu.au

different in size and external appearance, suggesting that they have different functions.

In addition to their location, dragonfly ocelli possess a number of unusual features. One such feature, common to both median and lateral ocelli, is that visual stimulation of these eyes evokes robust and pronounced head attitude reflexes (Stange and Howard 1979; Stange 1981). In the dragonfly *Hemicordulia tau*, a light-stimulus applied to the median ocellus causes the head to rotate forwards around the pitch axis, towards the light source. Stimulation of either lateral ocellus evokes corresponding head rotations around the roll axis. Ocellar driven head roll reflexes have also been demonstrated behaviourally in locusts (Taylor 1981), and ocellar inputs have recently been shown to act synergistically with input from compound eye movement detectors in tangential neurons encoding roll motion in the blowfly (Parsons et al. 2006).

Another unusual feature of the dragonfly ocelli is the presence of spatial resolution. With few exceptions, insect ocellar lenses have consistently been found to be profoundly underfocussed with respect to the retina (Homann 1924; Parry 1947; Cornwell 1955; Wilson 1978; Schuppe and Hengstenberg 1993), which immediately eliminates the possibility of high-resolution form vision at the level of individual photoreceptors. In addition, a characteristic feature of the dorsal ocelli is enormous input convergence from photoreceptors to second-order neurons (reviewed in Goodman 1981). In the somewhat extreme case of the cockroach, 10,000 photoreceptors converge onto just four second-order neurons (Weber and Renner 1976), making the convergence ratio somewhere between 2,500 and 10,000 (Mizunami 1994). The combination of these two factors is commonly considered to prevent retinotopic mapping of the world by second-, or higher-order interneurons of the dorsal ocelli.

However, recent studies have found that the ocelli of a number of insects are capable of some degree of form vision. Despite severe underfocussing, the ocellar lenses of the blowfly (Schuppe and Hengstenberg 1993), and the locust (Berry et al. 2007b), permit limited spatial resolution at the level of the retina. Warrant et al. (2006) have shown that the ocellar lenses of both diurnal and nocturnal paper wasps form focal planes either within, or just beyond, the proximal limit of the retina. Based on these observations, it would appear that the ocelli of these insects possess a modicum of resolving power.

Ophthalmoscopic examination of the median ocellus of the dragonfly *H. tau* also suggested that this ocellus is capable of substantial resolving power. Stange et al. (2002) found that a parallel beam of light shone into

the median ocellus is reflected back as eyeshine over a narrow range of incidence angles, implying that the incident light was well focussed by the ocellar lens onto the reflecting tapetum. Recent work has verified that the dragonfly median ocellar lens forms a focal plane within the retina, at a location that results in optimal resolution for individual photoreceptors (Berry et al. 2007a). Utilising single cell electrophysiology, van Kleef et al. (2005) found median ocellar photoreceptors to have elliptical receptive fields, with mean acceptance angles 15° wide in elevation, and 28° wide in azimuth. Given that the total field of view is approximately $120^\circ \times 60^\circ$ (Stange et al. 2002), it is estimated that the eye is capable of resolving a total of 16 pixels.

Recent work in our laboratory (Berry et al. 2006) has also shown that spatial information present in the outputs of median ocellar photoreceptors is retained after input convergence onto large second-order ocellar neurons (L-neurons). In total, 11 L-neurons are present in the median ocellar nerve, each mapping a distinct and restricted region of visual space. The form of the mapping is unusual in that, taken together, the L-neurons form a one-dimensional image of the external world that is extended in azimuth, but restricted in elevation. Given the differences in the external appearance of the median and lateral ocelli, it is of high interest whether this one-dimensional imaging arrangement is also preserved in the lateral ocelli.

In contrast to the median ocellus of the dragonfly, relatively little is known about its lateral ocelli. The fine structure of the dragonfly lateral ocellar retina and plexus has been previously described by Ruck and Edwards (1964) and also briefly by Rosser (1974). Morphological and optical details of the lateral ocellar lenses have not been described. The lateral ocelli have, however, been the subject of several investigations by extracellular electrophysiology (Ruck 1961a, b; Ruck and Edwards 1964; Rosser 1974; Kondo 1978), as the long lateral ocellar nerve lends itself to this purpose. The only intracellular recordings from the lateral ocellar nerve, were provided by Simmons (1982a), who also records from the median ocellar nerve and does not discriminate between the two. Chappell et al. (1978) provide the only known information about the morphology of L-neurons innervating the lateral ocelli. By cobalt iontophoresis of the ligated ocellar nerves, these authors described the proximal terminations of four large fibres, which exit the ocellar nerve and terminate in either the ipsilateral, or contralateral posterior slope (PSL). The dendritic arborizations and spatiotemporal properties of dragonfly lateral ocellar L-neurons remain unknown.

In order to determine the extent to which spatial resolution is preserved and utilised by the dragonfly lateral ocelli, this study examines these eyes on several levels. The previously undescribed structures of the lateral ocellar lens and associated retinal surfaces are determined by traditional histological methods and three-dimensional reconstruction. The location of the focal plane of the ocellar lens is determined by the use of the hanging-drop technique, in which an excised lens is suspended in a droplet of physiological saline such that the image formed by the lens can be directly observed. The quality of the image formed by the lens is assessed by determination of its modulation transfer function (MTF). MTFs are determined over a range of distances that covers the entire scope of the retina, allowing a complete description of the performance of the lens at any physiologically relevant location. The properties of lateral ocellar L-neurons are investigated by intracellular electrophysiology. L-neuron morphology is determined by a combination of fluorescent dye injection and confocal microscopy. Receptive fields of the L-neurons are determined in a physiologically relevant manner by the use of white noise analysis from a wide field, two-dimensional, bi-colour, LED display. The results are compared to known data from the median ocellus of the same animal.

Materials and methods

Experimental animals

Histology and electrophysiology were performed on adult dragonflies of the species *H. tau*. Dragonflies were either caught locally in Canberra, Australia, or reared to adulthood from larvae. Larvae were induced into emergence by relocation to a tank filled with warm (20°C) water, that was made slightly saline by adding an artificial sea salt mixture (Instant Ocean, 2 g/l), and regular feeding with blackworms (*Lumbriculus*) or water fleas (*Daphnia*). Adult dragonflies were typically stored in the dark at 4°C for a period of 1–3 days after capture or emergence before being used for electrophysiology or histology.

Histology

Fresh heads of *Hemicordulia* were partially dissected in fixative (3.7% formaldehyde, 2.5% glutaraldehyde in 0.01 M phosphate-buffered saline) by removing the mouthparts, frons and cuticle from the back of the head. Samples were then postfixed in 1% phosphate-buffered osmium tetroxide, dehydrated through a

graded alcohol series, and finally embedded in either a hard Araldite 502 resin or a soft Araldite 502/Epon 812 mix. Fixation, dehydration and infiltration times were often greatly reduced by microwave radiation (Pelco BioWave 34700–230). Semi-thin sections of 1 µm thickness were cut from hard Araldite 502 blocks on a Reichert-Jung type ultra-microtome. Thick sections of 15–30 µm thickness were cut from soft Araldite 502/Epon 812 blocks on an AOC Spencer 820 rotary microtome. Sections were post-stained with toluidine blue and imaged on a Zeiss Axioskop with a SPOT RT digital camera (1,024 × 1,300 pixels).

Measurement of focal length and image quality

Optical experiments are based on the hanging-drop method originally described by Homann (1924). Schuppe and Hengstenberg (1993) developed a method to describe the optical quality of a lens at various points of defocus behind the inner lens surface. The work presented here uses a modified version of their experimental setup, and has also been used to describe the imaging power of the dragonfly median ocellus and locust ocelli at physiologically relevant locations (Berry et al. 2007a, b). The imaging quality of lateral ocellar lenses was assessed by determining the MTF of the lens at various points of defocus behind the inner lens surface. The range of distances at which MTFs were determined covers the entire scope of the retina.

Ocellar lenses were dissected out from the head capsule, cleaned gently with a soft brush, then placed onto a drop of physiological saline (105 mM NaCl, 1.5 mM KCl, 0.9 mM CaCl, 2.4 mM NaHCO₃), which was suspended on a glass coverslip. The lens was oriented so that the outer surface was surrounded by air and the inner surface by water. The coverslip was then inverted and placed onto a rubber o-ring which itself was attached to a glass slide. Vacuum grease was used to seal the edges between the rubber ring and the coverslip to create an evaporation proof chamber. The slide and chamber were attached to a Goodfellow micromanipulator, which was used in place of a microscope stage to translate the slide in the *x*, *y* and *z* directions. The image formed by the lens was visualised by observation through the imaging optics of a compound microscope, the condenser of which had been removed. Ocellar lenses were aligned such that the optical axes of the lens and microscope objective coincided as closely as possible.

An LCD monitor positioned 10.28 cm (effective infinity) below the microscope objective was used to display various object patterns to the specimen lens over a wide visual field. Using a 20× objective with a

numerical aperture of 0.4 allowed objects within $\pm 23.5^\circ$ of the optical axis of the objective to be imaged. The stimuli used were sinusoidally modulated black and green gratings of spatial wavelengths ranging from 0.5° to 10° . To test for possible astigmatic effects, gratings were oriented in one of two directions: vertically modulated, such that the contrast of the gratings varies with elevation, or horizontally modulated, such that contrast varies with azimuth. Because the object patterns were projected across a plane covering a large visual angle, the patterns were corrected to maintain constant angular size from the viewpoint of the lens. Images were collected on a Canon Powershot G2 digital camera using remote shutter operation.

The experimental procedure consisted of focussing the microscope objective at incrementally increasing distances behind the inner surface of the lens and collecting a series of images at each point. The series consisted of images of different wavelength gratings at two orientations (horizontally and vertically modulated). Uncompressed RGB images were transferred to a computer and the green channel of the image was isolated. When viewing a large area of the image space of the lens, as used here, light concentration into the optical axis results in an artificially high contrast (Berry et al. 2007b). This was remedied by high pass filtering, with the resulting intensity distribution of the filtered image closely approximating theoretical expectations (Campbell and Green 1965; Campbell and Gubisch 1966; Warrant and McIntyre 1993). The maximum (I_{\max}) and minimum (I_{\min}) pixel values from the filtered image were determined and used to calculate the contrast (m) present in the image by use of the Michelson equation:

$$m = \frac{(I_{\max} - I_{\min})}{(I_{\max} + I_{\min})}. \quad (1)$$

MTFs were generated from contrast values at each point of defocus behind the inner lens surface, and used to determine the spatial cut-off frequency of the lens at that location. The linearity of the camera in the mapping from intensity to greyscale values was checked by successively decreasing the intensity of a light source with neutral density filters and determining the mean greyscale value of the resulting green channel isolated image. The mapping was found to be nonlinear, therefore a calibration curve was constructed to correct measured greyscale values to linear greyscale values.

The back focal distances or BFD (the distance between the inner surface of the lens and the plane of best focus) were calculated by describing the spatial

cut-off frequency as a function of distance from the inner lens surface, and defining the BFD as the location of maximum acuity. BFDs calculated in this way corresponded closely to BFDs calculated by directly observing the distance shift required to move the focus of the microscope objective from the inner surface of the lens to the plane of best focus. Note that distances must be multiplied by the refractive index of the immersion medium (1.34) to obtain a correct distance reading. The focal length (f) of each lens was also directly determined by calculating the transverse magnification of the lens using the formula:

$$f = s \frac{\lambda_i}{\lambda_o}, \quad (2)$$

where s is the distance between a test object and the lens, λ_o is the size of the object and λ_i the size of the corresponding image at the focal plane.

Electrophysiology

The experimental procedure used for determination of receptive fields of the lateral ocellar L-neurons follows closely from that used to analyse the spatiotemporal properties of L-neurons of the median ocellar nerve (Berry et al. 2006).

Dragonflies were secured with Periphery wax (Surgident) to a wax-covered rod, with the ventral side facing upwards and tilted towards the viewer at an angle of 45° . Recordings from the lateral ocelli were obtained by rotating the animal 55° in azimuth in order to expose the lateral ocellar nerve that runs dorsal to the median ocellar nerve plexus. The legs were immobilised with black insulation tape. The lateral ocellar nerves and ventral aspect of the brain were exposed by making a horizontal incision just anterior to the compound eyes to remove the frons and labrum. Air sacs overlying the ventral aspect of the brain were gently removed and the entire brain was bathed in dragonfly saline (same as above). The mandibles were waxed together to minimise movement within the head capsule.

A silver chloride wire, used as the indifferent electrode, was inserted directly adjacent to one of the lateral ocellar nerves. Microelectrodes were pulled by a P-87 Flaming/Brown Micropipette puller from thin walled 1.0–0.78 mm borosilicate glass (SDR Clinical Technologies). Electrode tips were filled by capillary action with 10% Lucifer Yellow CH (Sigma Chemicals) in 1% LiCl solution and then backfilled with 1 M LiCl. The output from the electrode was passed through a Getting 5A preamplifier, observed on an

oscilloscope and recorded on computer. Electrodes were fastened to a Leitz micromanipulator and advanced through the ventral surface of the lateral ocellar nerve until a sudden drop in voltage of 40–50 mV was encountered. The electrode was considered to be intracellular if the response to a sudden flash of light was similar to those of dragonfly L-neurons described previously (Chappell and Dowling 1972; Patterson and Chappell 1980; Mobbs et al. 1981; Berry et al. 2006).

A two-dimensional wide field LED display, described in Berry et al. (2006), was used for white noise analysis here. Briefly, the stimulus consisted of nine columns of LEDs, with each column containing 12 side-by-side pairs of green and UV LEDs (Roithner Lasertechnik). Each column of LEDs is driven by a pair of 14-bit D/A converters (Analog Devices AD5532HS), which themselves receive input from a Pentium-based computer via a microcontroller (Isopod, NewMicros). The stimulus has a refresh rate of 625 Hz, higher than that which the dragonfly ocelli can resolve (Ruck 1958). Concurrently active LEDs have a maximum intensity of $\sim 10^{14}$ photons $\text{cm}^{-2} \text{s}^{-1}$, which matches an equivalent patch of daylight sky.

In total, the stimulus consists of 216 LEDs arranged on the surface of a sphere of radius 120 mm. The head of the dragonfly was positioned at the centre of the sphere by locating it at the point of intersection of two aligned laser pointers. From this location the display covers 66° in elevation and 96° in azimuth. The total field of view of the lateral ocelli extends approximately 120° in elevation and 80° in azimuth (Stange et al. 2002). As it was not possible to orient the dragonfly such that the long axis of the stimulus extended in elevation rather than azimuth, the dragonfly was oriented so that the centre of the stimulus lies on the equatorial plane (elevation of zero), at an azimuth of 55° , with respect to the long body axis of the dragonfly. Oriented in this way, the wide field stimulus covered the ventral field of view of the lateral ocellus, and almost one half of the field of view of the median ocellus (as given by Stange et al. (2002)). A schematic diagram of the setup used is shown in Fig. 1. For the majority of L-neurons in the lateral ocellus, this setup was deemed to provide adequate coverage of receptive fields. Recordings were obtained from the lateral ocellar nerve, typically at a point close to where the nerve enters the brain.

Receptive fields were determined by recording the responses of a neuron to pseudorandom contrast patterns at times $t_n = n\Delta t$, where $\Delta t = 1.6$ ms and $n = 0, \dots, 25,023$. At each location the contrast values were uniformly and independently distributed in the range ± 0.82 . The cell response $y(\text{mV})$ to this sequence was

recorded, and the first-order space-time Wiener kernels (receptive fields) $h(t, \theta, \varphi)$, which describe the cell's linear temporal response to a contrast stimulus at each point of elevation (θ) and azimuth (φ), were obtained by fitting this response to the following equation using multiple linear regression (James et al. 2005; van Kleef et al. 2005).

$$y(t_n) = f_0(t_n) + \sum_{\tau=0}^{\tau_m} \sum_{\theta=-33}^{33} \sum_{\varphi=-48}^{48} h(\theta, \varphi, \tau) \cdot c(\theta, \varphi, t_n - \tau). \tag{3}$$

In Eq. 3 f_0 includes a constant offset, a term that removes low frequency drift as fitted by a fifth order polynomial, and a term that removes 50 Hz hum as fitted by a periodic function (van Kleef et al. 2005). The contrast at each point of elevation and azimuth is defined as $c = (I - I_0)/I_0$, where I is the intensity level at that point and I_0 is its mean temporal intensity. The optimal memory of this model (τ_m) was obtained using the cross-validation methods outlined in van Kleef et al. (2005). The receptive field was taken to be the spatial profile that occurs at the time step when the maximal value of h occurs.

Visualisation of stained neurons

Upon successful completion of an intracellular recording, units were identified with Lucifer Yellow by iontophoretic injection of 5–10 nA negative current, for a period of up to 60 min. Following current injection, the brain and suboesophageal ganglion were dissected in fixative (3.7% paraformaldehyde in phosphate buffered saline), transferred to 3.7% formaldehyde in methanol for 45 min, dehydrated through an ethanol series and mounted in methyl salicylate. Filled neurons were observed under a Nikon Optiphot epifluorescence microscope. When the quality of the filled neuron was acceptable, the preparation was optically sectioned on a Leica SP2 UV confocal microscope.

Results

General orientation

In *Hemicordulia* and many other Anisoptera, the ocellar triangle and antennae are located within a tight space above the mouthparts. The centrally located median ocellus is strongly elliptical and lies recessed into a groove between the frons and the vertex (Fig. 2).

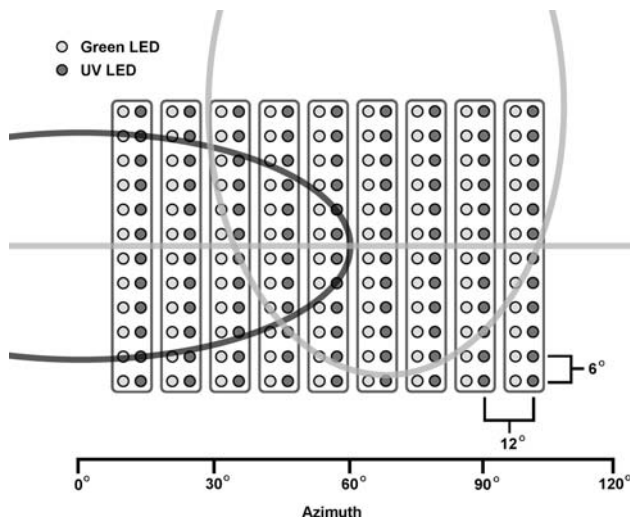


Fig. 1 Schematic diagram of the wide field LED display used for white noise analysis of lateral ocellar L-neurons. The display consists of nine columns, each column containing 12 rows of green and UV LED pairs. Resolution is higher in the vertical direction (6°) than the horizontal direction (12°) to match the receptive fields of photoreceptor neurons in the median ocellus (van Kleef et al. 2005). The head of the dragonfly is oriented such that the display covers as much as possible of the lateral ocellar field of view (*light grey ellipse*) as well as half of the median ocellar field of view (*dark grey ellipse*). The centre of the display lies on the equatorial plane (*grey line*), at an elevation of 0° and at an azimuth of 55° . Note that the figure is a schematic projection, with angular distances depicted as constant size. In reality, LEDs are arranged around the surface of a sphere of radius 120 mm

The optical axis of the median ocellus lies approximately parallel with the long body axis of the dragonfly in level flight (Stange et al. 2002).

The smaller lateral ocelli are located on either edge of the vertex (Fig. 2) and are bounded posteriorly by the very large and prominent compound eyes. They lie slightly dorsal and anterior to the median ocellus. In level flight, the field of view of the median ocellus lies close to centred on the horizon. Lateral ocellar fields of view are elliptical, extending across 80° of visual space in azimuth and 120° in elevation. Fields of view are centred dorsally at elevations of approximately 30° , and laterally at azimuths of $\pm 80^\circ$ (Stange et al. 2002).

Histology of the dragonfly lateral ocelli

The lateral ocellar lens

The outer surface of the lateral ocellar lens of *Hemicordulia* is hemispherical, with an aperture of approximately $300\ \mu\text{m}$ in both the horizontal (transverse) and vertical (coronal) planes. The radius of curvature is uniform, with a spherical radius of approximately

$240\ \mu\text{m}$. The inner surface of the lens is of a geometrically complex shape, somewhat resembling a boot. This shape is most evident from reconstructions of the lens (Fig. 3), and from sections taken in the vertical plane (Fig. 4). Anteriorly, the inner surface appears continuous and the entire lens appears roughly plano-convex; the inner surface is flat (Fig. 4a). Further posteriorly, the dorsal half of the inner surface begins to protrude inward. At this level (Fig. 4b, c), two distinct inner surfaces are clearly visible from cross sections of the lens. The dorsal surface is more strongly curved than the ventral surface, with a radius of curvature of approximately $280\ \mu\text{m}$. It should be noted, however, that this is a coarse approximation, as the surface is not uniformly circular, being more strongly curved near the midline of the lens.

Retinal structure and relationship to lens

The neural constitution of the lateral ocellar retina appears to be identical to that of the median ocellus (Stange et al. 2002; Berry et al. 2007a). Triad shaped rhabdoms form at the junction of three retinula cells, and dense brown pigment can be observed cupping the proximal bases of the rhabdoms in thick sections of the eye (Fig. 4c). By analogy with the median ocellus (where a similar pigment is also observed) this layer is presumed to be reflective, and ensheathes between one-third and one-quarter of the rhabdom length. Rhabdom tips are located almost directly behind the inner lens surface and have circular diameters of approximately $4.5\text{--}7\ \mu\text{m}$. Rhabdoms enlarge proximally, where circular diameters range from 13 to $16\ \mu\text{m}$. Rhabdoms are somewhat irregularly arranged throughout the retina, but are well separated by 14 to $20\ \mu\text{m}$ from their nearest neighbours.

As the lens of *Hemicordulia* is split into ventral and dorsal segments, so too is the retina (Figs. 3, 4). In level flight, the orientation of the lens is such that the dorsal retinal surface appears to be oriented to receive light from around the equator, and slightly forward from 90° in azimuth. The ventral surface is directed dorsally, and slightly backwards from 90° in azimuth.

Rhabdoms of the two retinæ differ in their structural arrangement. Within the ventral retina, rhabdoms are of approximately constant length, extending proximally for a distance of $90\text{--}100\ \mu\text{m}$. The dorsal retina shows a parabolic distribution of rhabdom length in the vertical plane. In this case, rhabdom lengths are approximately $80\ \mu\text{m}$ near the dorsal and ventral extremes of the retina, and reach a peak of $220\ \mu\text{m}$ near the centre of the retina. This arrangement directly resembles that found in the median ocellus, where

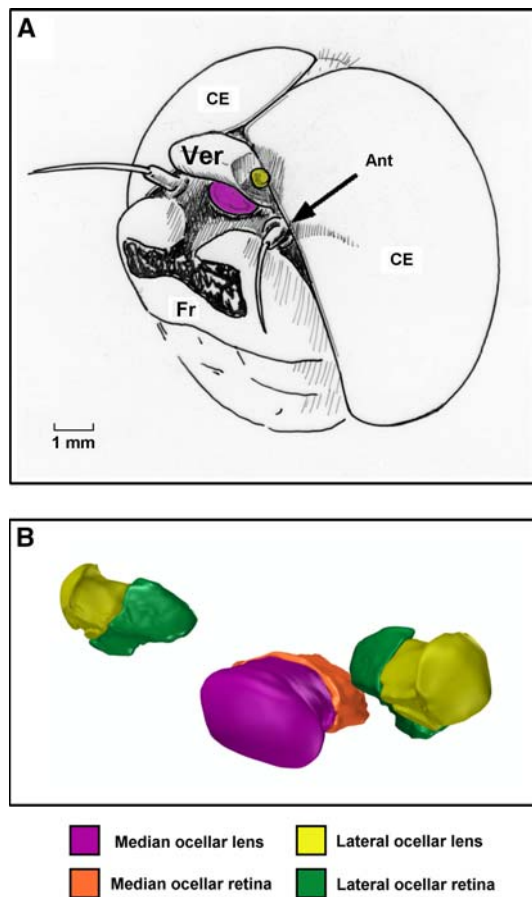


Fig. 2 Drawing (a) and three-dimensional reconstruction (b) displaying the locations of the ocelli in the dragonfly *Hemicordulia*. The median ocellus is recessed into a cuticular groove above the frons (*Fr*) and below the vertex (*Ver*). The elevational field of view of the median ocellus is constrained by these structures. Lateral ocelli sit on the outer edges of the vertex and lie slightly anterior to the median ocellus. Their fields of view are partially constrained by the antennae (*Ant*) and the anteromedial borders of the compound eye (*CE*). Drawing in a has been adapted from Stange (1981). Note that only one lateral ocellus was reconstructed, the other is a mirror copy

rhabdom length also differs over very similar proportions across the vertical plane (Stange et al. 2002; Berry et al. 2007a).

Photoreceptor axons project through a thick, pigmented sheath that surrounds and defines the retina and thereafter form a synaptic zone with the second-order interneurons. The plexus area does not form a well-defined region, but instead tapers into a relatively thin nerve fibre that runs adjacent to the median ocellar nerve. The lateral ocellar nerves are much longer, thinner, and more cylindrical than the median ocellar nerve. All three nerve tracts enter the brain at approximately the same level, with the lateral ocellar entering laterally to the median ocellar nerve.

Dioptrics of the lateral ocellar lens

Imaging by the excised lens

Gratings and other simple stimuli were imaged through isolated lateral ocellar lenses to determine a number of properties of the lens, and these are summarised in Table 1. The image produced by the lens was consistently of good quality, and no evidence of astigmatism was found; the location of the focal plane does not differ for stimuli of different orientations (two-tailed *t*-test, $P < 0.05$). Combining the results from both vertically and horizontally modulated stimuli yielded an average BFD of $96 \mu\text{m}$ behind the most proximal point of the lens (Fig. 5).

The quality of the image formed by the lateral ocellar lens is also independent of the orientation of the stimulus. As shown in Fig. 6, the shape and peak spatial cut-off frequencies are similar for both vertically and horizontally modulated gratings, and no significant differences between the two were found (two-tailed *t*-test, $P < 0.05$). Modulation transfer functions determined from vertically or horizontally modulated gratings at the focal plane of the lens yielded spatial cut-off frequencies of 1.06 and 0.99 cycles/degree, respectively (Fig. 6). These values are comparable to values obtained from dragonfly median ocellar lenses (Berry et al. 2007a). The steep slopes of the curves indicate that the image comes into sharp focus at the focal plane, and this was verified by direct observation.

Note, however, that the resolving powers of the ventral and dorsal retinae are critically dependent on their locations within the eye. The dorsal surface of the lens acts an optical spacer, such that the dorsal retina is located much closer to the focal plane of the lens than the ventral retina (Fig. 5). As most of the ventral retina lies distal to the dorsal surface of the lens, this retina must receive a poorly focused image from the optics (Fig. 5). From analysis of MTFs determined $25 \mu\text{m}$ proximal to the inner lens surface (the shortest distance from the lens analysed), the spatial cut-off frequency is only 0.38–0.42 cycles/degree and increasing rapidly with increasing distance from the lens (Fig. 6). Therefore, while spatial frequencies of up to 1.06 cycles/degree are theoretically resolvable by the lens, this level of resolution could only be achieved by the dorsal retina; the ventral retina must have significantly lower resolving power.

Theoretical description

As the inner surface of the lens consists of distinct dorsal and ventral components, it was initially expected

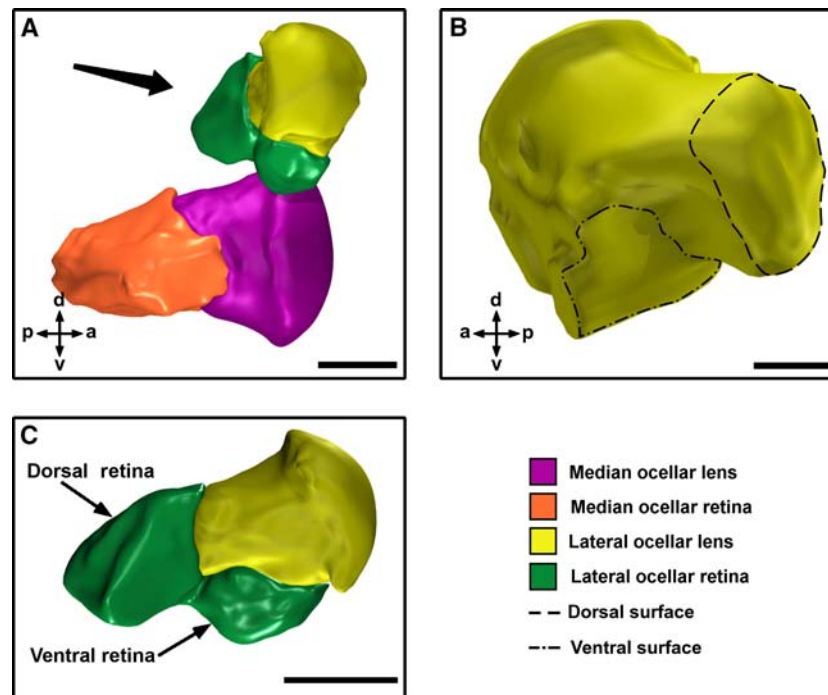


Fig. 3 Three-dimensional reconstructions of the dragonfly ocelli generated from serial sections of *Hemicordulia*. **a** Lateral view of the median and right lateral ocelli. *Thick arrow* indicates the approximate direction from which the image in **c** was obtained. **b** Rear view of the lateral ocellar lens. **c** Posterior and slightly dorsal view of the lateral ocellar lens with retina. Note the pronounced protrusion that forms the dorsal lens surface. The

dorsal retina attaches to this surface with a field of view centred just above the equator and slightly forward of 90° azimuth. The smaller ventral retina attaches to the ventral surface of the lens with a field of view centred dorsally and slightly backwards of 90° azimuth. *Small arrows* in **a** and **b** indicate body axes: *d* dorsal, *v* ventral, *a* anterior, *p* posterior. Scale bars: **a**, **c** 200 μm; **b** 100 μm

that the inner surfaces might have differing refractive powers, thus forming images in two locations. However, little evidence for dual focal planes was observed. Some effect of inner surface refraction may be evident in regions of the image showing lower contrast (see for example the upper regions of images shown in Fig. 5a, b), but such variation was typically small. Different regions of the image could not be consistently related to differences in the underlying geometry of the lens, such that one of the inner lens surfaces could be said to result in a longer focal length than other. From section data (Fig. 4) it can be seen that the inner surfaces of the lateral ocelli are relatively flat with respect to the outer surface. From calculations of the focal length of the lens using standard thick lens formulae (see Land 1981), it is estimated that the inner surfaces account for only 5–17% of the total refractive power of the lens, and are therefore largely ineffective as a refractive interface.

Additionally, assuming a refractive index value of 1.5, and calculating the focal length of the lens from its radii of curvature yields a focal length of 410 μm. This is 1.8 times longer than measured focal lengths as determined directly by the transverse magnification of objects imaged through the lens. This discrepancy may

be accounted for if the refractive index of the lens is not homogenous, but instead is graded such that the centre of the lens is of higher refractive index than the periphery. We have recently given direct evidence by interference microscopy that the dragonfly median ocellar lens contains such a refractive index gradient, and in this case theoretically determined focal lengths are similarly much longer than actual focal lengths (Berry et al. 2007a). It appears likely that the refractive index of the lateral ocellar lens is graded in a similar manner to the median ocellar lens.

The short focal length and wide aperture of the lens results in a low *F*-number of 0.78. In combination with long and thick photoreceptors, this suggests that the eye is adapted for exceptionally high sensitivity. The optical sensitivity (*S*, in units of μm² sr) of an eye in broad-spectrum light is given by:

$$S = \left(\frac{\pi}{4}\right)^2 A^2 \left(\frac{d}{f}\right)^2 \left(\frac{kx}{2.3 + kx}\right), \quad (4)$$

where *A* and *f* are the aperture and focal length of the lens respectively, *d* is the diameter of the rhabdom, *x* is its length, and *k* is the absorption coefficient (Warrant

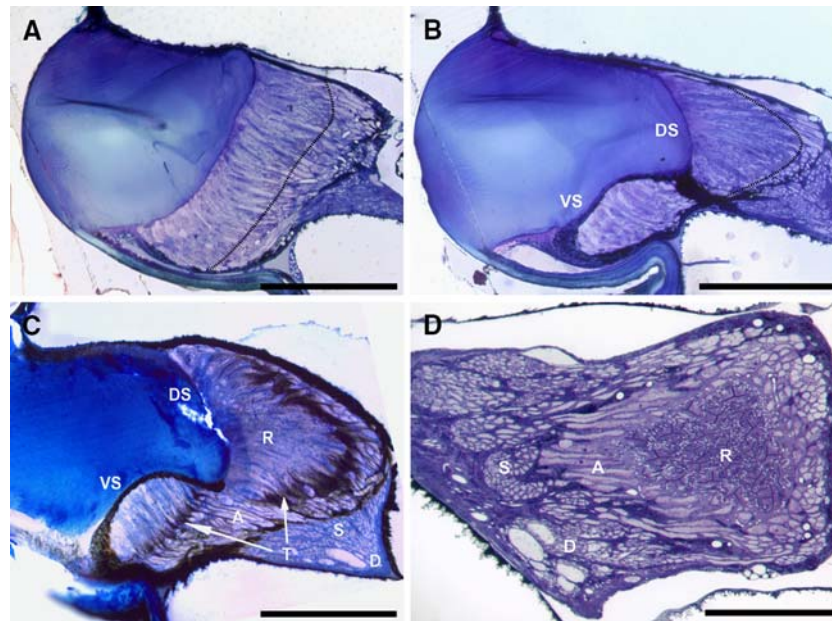


Fig. 4 Light micrographs of the lateral ocellus of *Hemicordulia*. Sections in **a**, **b** and **c** are taken in a vertical orientation through the lens and retina. Section in **a** is taken anterior to section in **b**. The inner surface of the lens appears continuous at this point, rhabdom length is relatively short and does not change across the retina. Further posterior, at the level of **b**, the dorsal (DS) and ventral (VS) surfaces of the lens become visible. Retinula cells are attached to each surface. In the dorsal retina, rhabdom length changes approximately parabolically in the ventral-dorsal direc-

tion. Section in **c** is taken at approximately the same location as **b**, but is a thick (20 μm) section, which allows visualisation of tapetum (T) ensheathing rhabdom bases. A frontal section through the distal retina is shown in **d**. Triad shaped rhabdoms are visible and are of similar proportions as in the median ocellus. R Rhabdoms, A Retinula cell axons, S Synaptic plexus zone, D Dendrites of second-order neurons. Dashed lines in **a** and **b** indicate proximal limit of rhabdoms. Scale bars: **a–C**: 200 μm; **d** 50 μm

Table 1 Optical properties of the lateral ocellar lens as obtained from six preparations of *Hemicordulia*

Parameter	Plane	<i>Hemicordulia</i> (lateral ocellus)
Aperture (μm)	Horizontal	300
	Vertical	299
Focal length (μm)	Horizontal	238 ± 23
	Vertical	228 ± 30
BFD (μm)	Horizontal	98 ± 22
	Vertical	93 ± 33
V_c (cycles/degree)	Horizontal	0.99 ± 0.39
	Vertical	1.06 ± 0.25
F -number		0.78
Optical sensitivity (μm ² sr)		26

Values are given as mean ± standard deviation where possible. Values for spatial cut-off frequency (V_c) were obtained from the focal plane of the lens. In no case were significant differences found between the horizontal and vertical planes ($P < 0.05$)

and Nilsson 1998). Using the values given in Table 1, with a mean receptor diameter of 8 μm, a maximum receptor length of 220 μm, and an absorption coefficient of 0.0067 μm⁻¹, yields an optical sensitivity value of 26 μm² sr. For comparison, similar calculations from the apposition eyes of the dragonflies *Sympetrum striolatum* and *Sympetrum vulgatum* result in optical sensitivities of

just 0.29–1.7 μm² sr (Labhart and Nilsson 1995). Dragonfly lateral ocelli are also some 3.9–5.8 times more sensitive than locust ocelli ($S = 4.5–6.6$ μm² sr), but of comparable sensitivity to the median ocellus of *Hemicordulia* ($S = 31.5$ μm² sr) (Berry et al. 2007a).

Anatomical profiles of individual L-neurons

The results described below are based on over 60 recordings of L-neurons from one of the two lateral ocellar nerves of *Hemicordulia*. Of these, 15 L-neurons were successfully identified by iontophoretic dye injection. In combination with receptive field analysis this allowed the classification of four types of L-neuron. The naming convention used here is based on the original scheme provided by Chappell et al. (1978) for the lateral ocellus, and this scheme has also been used to describe the L-neurons of the median ocellus (Patterson and Chappell 1980; Mobbs et al. 1981; Berry et al. 2006). A neuron is referred to as ipsilateral if its axon terminates in the same side of the brain as the lateral ocellar nerve it innervates. Conversely, if the axon crosses midline to terminate in the opposite half of the brain, it is referred to as contralateral.

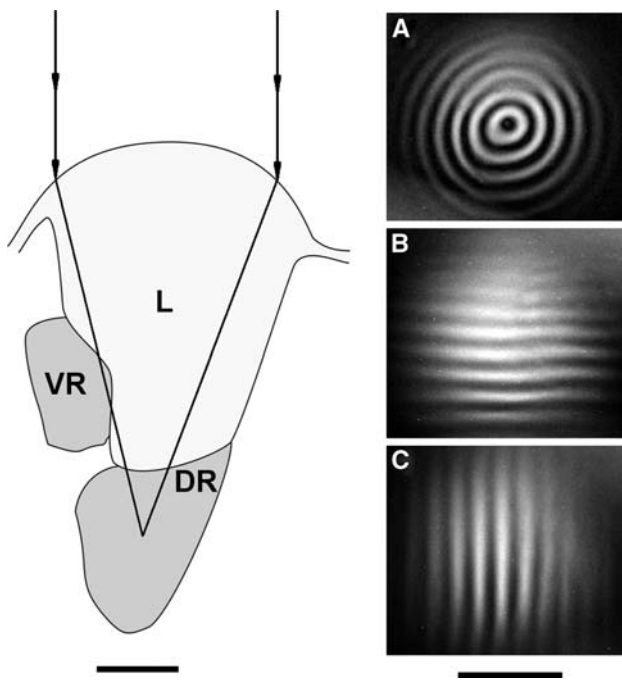


Fig. 5 Schematic representation of focal plane location in the lateral ocellus of *Hemicordulia*. Outline of lens (*L*) and retinae were traced from a vertical cross-section of the eye at a location where ventral (*VR*) and dorsal (*DR*) retinae are visible (see Fig. 4b). Focal plane is shown at the location of convergence of two parallel rays. A radial pattern (**a**), as well as vertically (**b**) and horizontally (**c**) modulated gratings of 5° spatial wavelength imaged through the lens at the focal plane are shown on the right. Scale bars: all $100\ \mu\text{m}$

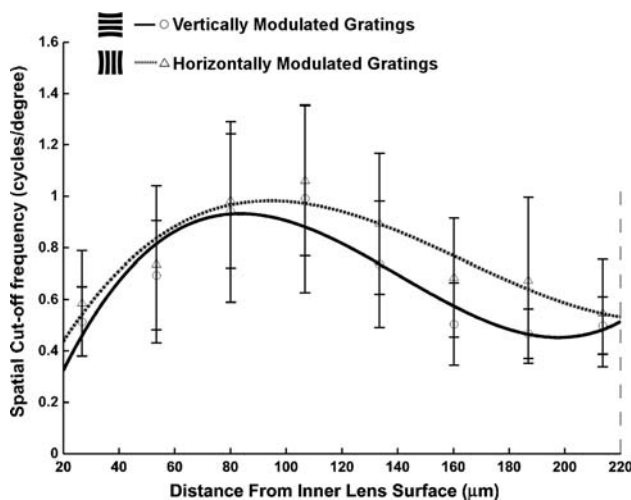


Fig. 6 Spatial cut-off frequency functions of the lateral ocellar lens. The spatial cut-off frequency of the lens is given at various points of defocus behind the inner lens surface. The lens is stigmatic and image contrast is independent of stimulus orientation. Legend indicates the orientation of the stimulus used. Dashed line indicates proximal limit of rhabdoms

LI₁ and LI₂

By mass staining ligated lateral ocellar nerves with cobalt, Chappell et al. (1978) identified and described the proximal terminations of two LI (lateral, ipsilateral) cells present in each lateral ocellar nerve of *Aeschna tuberculifera* and *Anax junius*. Here we similarly confirm the presence of two LI cells in the lateral ocellar nerves of *Hemicordulia tau* and provide some details of the hitherto undescribed dendritic arborizations of these neurons.

The morphology of both LI cells is very similar, and generally these neurons could not be distinguished by anatomy alone (Fig. 7a, b). They were, however, easily identified by receptive fields, which differ drastically between the two cells. Proximal to the ocellar plexus, these neurons collate to form thick axonal trunks of $10\text{--}20\ \mu\text{m}$ diameter, which run the length of the long lateral ocellar nerve without bifurcation. After entry into the brain, these neurons first run towards the midline, before turning back to run in a posterolateral direction through the ipsilateral protocerebrum. Like most ocellar L-neurons, these neurons run along the dorsal-most aspect of the brain and terminate in the posterior slope (PSL), a total length of nearly $1.2\ \text{mm}$. The cell bodies of all L-neurons are located either within, or adjacent to, the pars intercerebralis. Cell bodies are connected to their respective axons by slender neurites, which run posteromedially before looping back to join the axon.

Chappell et al. (1978) describe the axons of both LI neurons as running in close association with each other, with one of the two running in a slightly more lateral position, and terminating in a more lateral region of the posterior slope (PSL). The nomenclature provided by Chappell et al. (1978) denotes more medial neurons by a lower subscript (LI₁ lies medial to and terminates in a more medial location than LI₂). However, the location of a stained neuron with respect to other unstained neurons is difficult to determine where single cell staining rather than mass staining techniques are employed. Therefore we assign the lowest subscript to the neuron with the most medial receptive field. Both neurons terminate in close proximity to, but slightly more lateral than, the most lateral of the median ocellar L-neurons (MI₂).

LI₁ is typically of slightly larger axonal diameter than LI₂, however, axon diameter may vary markedly throughout the course of the nerve. Additionally, the dendritic arborizations of LI₁ appeared more widespread than those of LI₂, which typically appear quite constricted. However, the dendritic arbours of LI₂ were often obscured by a strongly pigmented sheath



Fig. 7 Ventral views of stained lateral ocellar L-neurons from four different preparations of *Hemicordulia*. L-neurons were identified by iontophoretic injection of Lucifer Yellow after recording from the unit. **a** A double fill of LI₁ and LD, each recorded from a different lateral ocellar nerve. **b** The LI₂ neuron, which is anatomically similar to LI₁. **c** The tri-ocellar neuron MB. In this case the unit was recorded from the left lateral ocellar nerve, which is innervated by a slender collateral (*arrows*). Collateral innervating the right lateral ocellus did not stain in this

preparation. **d** Fine branching pattern of the LI₁ neuron in the lateral ocellar nerve. Dendritic terminals of this neuron are not restricted to the ocellar plexus; a series of short dendritic processes (*SDP*) are also visible over a long segment of the ocellar nerve (within range marked by *arrows*). With the exception of **c** all images are maximum intensity projections from a series of optical sections taken through the brain. **c** is an image taken under direct epifluorescence. Scale bar: all 200 μm

that encloses the retina and appears opaque under fluorescent excitation. One possible explanation for this difference is that LI₁ and LI₂ project to different regions of the lateral ocellar retina, which consists of dorsal and ventral components. It is suggested that the difficulty in visualising the dendritic arbours of LI₂ is due to this neuron projecting to the ventral retina, which is obscured by the overlying dorsal retina. Although an extensive effort was made to visualise the dendritic arbours of all lateral ocellus L-neurons, it was not possible to determine the extent to which any neuron innervated either of the two retinæ.

On two occasions, one of which is shown in Fig. 7d, LI₁ was observed to form a series of short, thin, dendritic processes which extend perpendicularly outwards from the main trunk of the axon (which is swollen to a

diameter of nearly 30 μm in this area), well within the ocellar nerve itself. Dendritic arborizations are normally confined to a relatively small region of the ocellar nerve just proximal to the retina: arborizations further down the ocellar nerve were not observed in any other neuron. However, this feature was only observed when intracellular staining was of very high quality, and such arborizations may have been present, but not observable, in other L-neurons. These dendrites are presumably contacting other second-order neurons, as the axons of photoreceptors do not appear to penetrate this far into the ocellar nerve. Direct evidence for connections between ocellar interneurons has been given by simultaneously recording from ocellar interneuron pairs in both the dragonfly (Simmons 1982a), and the locust (Simmons 1982b).

LD

The neurons referred to here as LD (lateral, descending) (Fig. 7a) have not been described previously. The LD neurons are morphologically distinct from other L-neurons of the lateral ocelli, but bear many similarities to the MD (median, descending) neurons of the median ocellus (Berry et al. 2006). Unlike other L-neurons, these neurons do not run along the dorsal-most aspect of the brain, nor do they terminate in the posterior slope. Instead, the 20–30 μm diameter axon proceeds through the middle of the brain, with the main trunk of the axon terminating in the ipsilateral posterior deutocerebrum or anterior tritocerebrum. Midway through the course of the brain, a slender process of 5–10 μm diameter is given off which curves around the suboesophageal foramen and enters the contralateral suboesophageal connective (Fig. 7a). The descending collateral of this neuron is known to enter the suboesophageal ganglion (SOG), but could not be traced further due to limitations in dye diffusion. From dendritic arborizations to the visible limits of the process entering the SOG, these neurons extend over a total length of at least 1.5 mm.

MB

The last of the four L-neurons innervating the lateral ocellar nerve is the single, unpaired neuron MB (median, bilateral), the morphology of which has been described in a previous study (Berry et al. 2006). Briefly, this neuron innervates the medial aspects of both lobes of the median ocellar plexus. The main axonal trunk runs down the centre of the brain before bifurcating into two large branches, each of which terminates in either the left or the right PSL. Soon after entry into the brain, this neuron gives off two slender processes which extend outward to innervate the left and right lateral ocelli. The processes innervating the lateral ocelli have a diameter of approximately 10 μm , which is half the size of the processes innervating the median ocellar nerve. Figure 7c gives an example of an identified MB neuron that was recorded from the lateral ocellar nerve.

Physiological responses to pulses of light

Time course

The wide field stimulus used here was primarily designed for analysis of receptive fields, but could also be used to display a simple light-on, light-off type stimulus. This type of stimulus is useful for identifying

when an L-neuron has been successfully impaled by an electrode, as L-neurons give characteristic and easily identifiable responses to light pulses (Chappell and Dowling 1972; Patterson and Chappell 1980; Mobbs et al. 1981; Simmons 1982a; Berry et al. 2006).

Figure 8a shows a typical response of an L-neuron to a pulse of light. A large transient hyperpolarization is observed approximately 10–12 ms after stimulus onset. The membrane potential of the cell then rebounds to a hyperpolarized plateau, which is maintained for the length of the stimulus. Soon after stimulus offset a fast depolarizing transient is observed, this rebounds quickly and may oscillate around the resting membrane potential of the cell before a slow depolarizing afterpotential occurs. Recorded units described here were required to show large (> 10 mV), stable responses to light pulses for approximately 2 min, with little fluctuation in resting membrane potential, before intracellular responses were recorded.

In contrast to L-neurons, which are physiologically defined by large graded potentials, units showing a distinctly different response to light pulses were occasionally encountered in the lateral ocellar nerve. These units were categorised by almost no graded response, but large regenerative potentials, which could be either excited or inhibited (Fig. 8c) by light. Judging by their instability these units were typically of smaller diameter than the L-neurons, and they are therefore presumed to be S-neurons. Their responses are entirely consistent with other intracellular and extracellular recordings of presumed S-neurons (for example Rosser 1974; Kondo 1978; Wilson 1978; Simmons 1982a). Attempts to identify these units by iontophoretic dye injection were unsuccessful.

Specific characteristics of LD

The LD neurons are distinct from other L-neurons of the lateral ocelli for the reason that, in addition to large graded responses, these neurons also produce regenerative potentials (Fig. 10b). LD neurons may be spontaneously active, with firing frequency reduced during light onset and increased at light offset, or they may produce regenerative potentials only following light offset. The spike initiation zone is sufficiently close to the site of recording to be affected by current injection, with the effect that negative current reduces, while positive current increases, the firing frequency of the cell. The physiological responses of LD are consistent with those of MD neurons in the median ocellus (Berry et al. 2006).

LD neurons sometimes changed response waveform throughout the recording period such that, for exam-

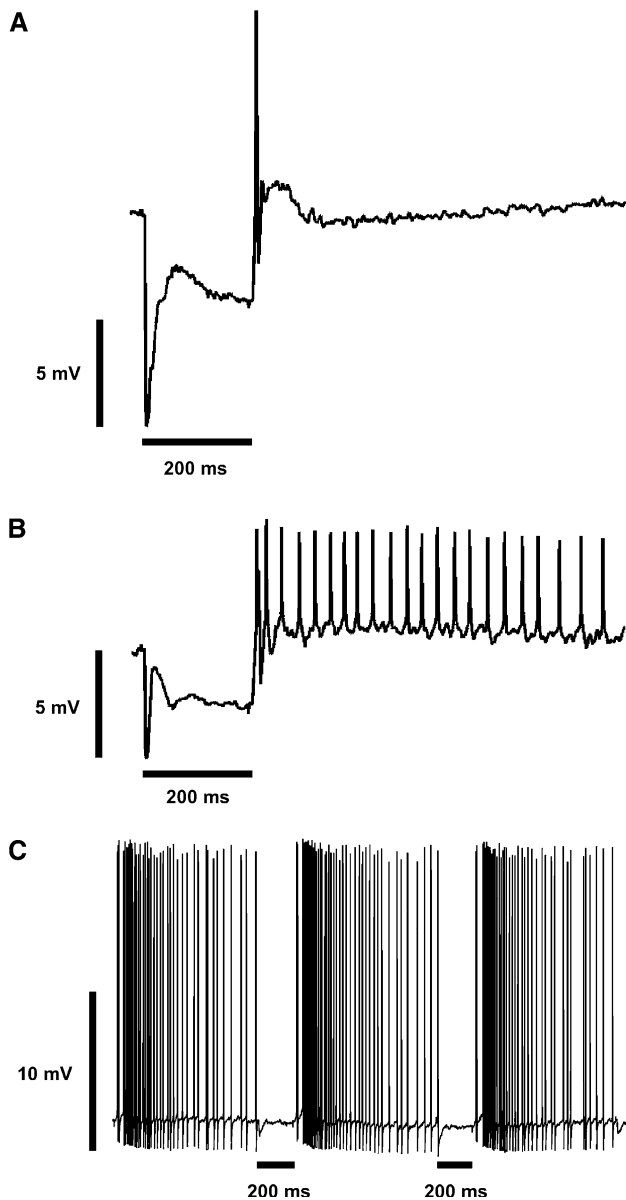


Fig. 8 Typical responses of ocellar interneurons to pulses of light. **a** shows the representative response of an L-neuron (LI_1) to a square wave UV light pulse of 200 ms duration. **b**, **c** show the responses of LD and a presumed S-neuron to the same stimulus

ple, a unit initially showing regenerative potentials reverted to the more classical response of other L-neurons where only graded potentials are observed. In no case, however, was an L-neuron of any other type found to produce regenerative potentials, which provides an easy means of identifying LD neurons physiologically.

Receptive fields by Wiener kernel analysis

Receptive field contour maps and acceptance angle outlines for representative examples of lateral ocellar

L-neurons are shown in Fig. 9. The procedure used to determine receptive field outlines is identical to those recently used in our laboratory to analyse the spatio-temporal properties of photoreceptors (van Kleef et al. 2005) and L-neurons (Berry et al. 2006) of the median ocellus.

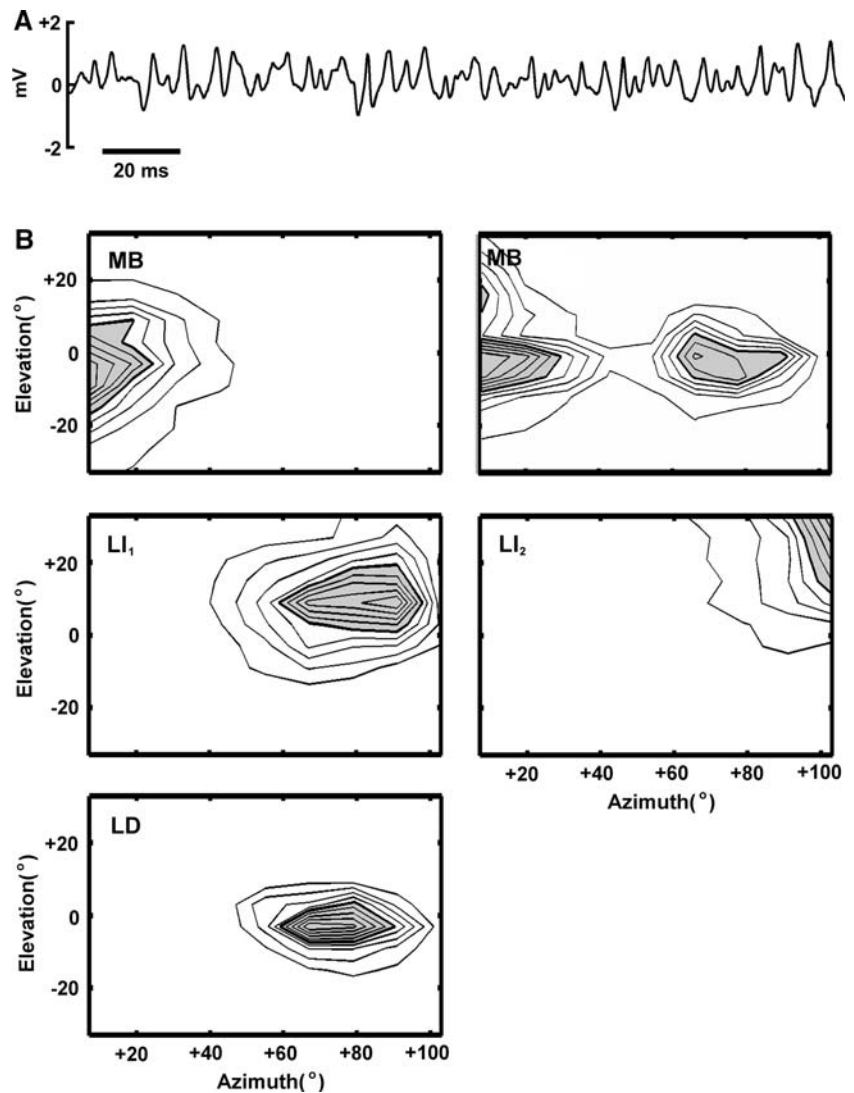
Receptive fields shown here are calculated from responses to pseudorandom modulation of UV light, taken at a delay that produced maximal response. With the exception of MB, maximum amplitude responses typically occurred 12–16 ms after stimulus onset. Maximum amplitude responses of MB occur at latencies of 20.8–22.4 ms after stimulus onset, suggesting that additional chemical pathways contribute to the response of this cell. We also calculated receptive fields from responses to UV stimulation in the presence of green light, as well as from responses to green light alone, but did not observe systematic differences in receptive field.

The receptive fields of LI_1 and LD are very similar, with a large degree of overlap occurring between the two neurons. The fields are elliptical, being approximately twice as wide in azimuth (34.1 – 29.7°) as in elevation (13.3 – 12.0°). The centre points of both receptive fields lie close to the equator, slightly forward of 90° in azimuth, suggesting input from the dorsal retina. Distinctly different is the receptive field of LI_2 . The receptive field of this neuron always exceeded the limits of the stimulus, and therefore only a partial description can be given. The centre point of this field lies at an azimuth greater than 103° , and at an elevation greater than 33° , suggesting input from the ventral retina. As it is not centred close to the equator, the receptive field of LI_2 is distinctly different from those of all other dragonfly L-neurons. Additionally, LI_2 is the only known ocellar L-neuron to be centred backwards of 90° azimuth.

Successfully identified recordings of the unpaired MB neuron were obtained twice from the lateral ocellar nerve. However, the results obtained from these two preparations differed significantly. In one preparation (shown on left in Fig. 9b), this neuron did not respond to stimulation of the lateral ocellus; the receptive field was constrained to a region of visual space that is viewed by the median ocellus only. In the other preparation (shown on right in Fig. 9b), one region of the receptive field occurred in the viewspace of the median ocellus, and another region occurred in the viewspace of the lateral ocellus. In this case, the receptive field in the lateral ocellar viewspace was of similar size and location as those of LI_1 and LD, being elliptical and centred close to the equator at an azimuth of 75° .

In general, receptive fields of the same neuron were found to be of a consistent size, and location, between

Fig. 9 a Representative response of a lateral ocellar L-neuron to the white noise stimulus used to determine receptive fields. **b** Examples of the obtained two-dimensional spatial receptive fields from all identified lateral ocellar L-neurons. All receptive fields are from the right lateral ocellus of the dragonfly. The dragonfly is oriented such that a large region of the lateral ocellar field of view is covered, as well as the right half of the median ocellar field of view (Fig. 1). Receptive field maps of two MB neurons obtained from different preparations are shown. Recording on left appears devoid of lateral ocellar input, while recording on right appears to receive strong input from lateral ocellus. Positive-going elevation values represent the upwards direction. Positive-going azimuth values represent the rightwards direction. Contour maps of the full receptive field are shown in *black outlines*, with responses at or above 50% of the maximum response shown shaded in *grey*



preparations. An indication of the amount of variability between recordings is given in Table 2. This gives the mean and standard deviations of centre point locations, and acceptance angles, averaged over all recordings of identified L-neurons. Centre point values in elevation show the largest variation, which is probably attributable to the difficulty of orienting the dragonfly for recording from the lateral ocellar nerves. In the setup used here, the dragonfly was oriented on an oblique angle, where small deviations in rotation about the long axis of the dragonfly have a large effect on elevation.

Discussion

Morphology and dioptrics

Investigation of the lateral ocellar lens and retinæ by standard histological techniques revealed some un-

sual properties of this eye. In particular, while the outer surface of the lens is continuous and strongly curved, the inner surface of lens contains a pronounced inwards protrusion, which divides the lens into dorsal and ventral components.

Dorsal and ventral retinal surfaces attach directly to each of the respective lens surfaces, and the two retinæ differ in their fields of view and resolving capacity. The majority of the retinula cells forms the dorsal retina, which is directed towards the equator, slightly forward of 90° in azimuth. The focal plane of the lens lies within the centre of this retina, close to the location where tapetal sheathing of rhabdom bases begins. However, rhabdoms in the dorsal retina become progressively shorter and increasingly underfocussed towards the dorsal and ventral extremes. A similar arrangement is found in the dragonfly median ocellus. In this case, ray tracing through the lens and retina demonstrates that such an arrangement results in

Table 2 Mean receptive field centre points and acceptance angles of L-neurons innervating the dragonfly lateral ocellus

Cell type	<i>n</i>	Centre point (degree)		Acceptance angle (degree)	
		Azimuth	Elevation	Azimuth	Elevation
LI ₁	5	76.6 ± 3.2	-1.3 ± 8.6	34.1 ± 4.4	13.3 ± 4.8
LI ₂	4	>103.0 ± 0.0	>33.0 ± 0.0	>12.2 ± 2.2	>19.2 ± 7.0
LD	4	77.6 ± 5.1	5.2 ± 7.4	29.7 ± 2.4	12.0 ± 2.5
MB	1	74.5	-4.8	31.9	14.8

Values were taken only from preparations in which the recorded unit could be clearly identified by anatomy. The number of recordings of each cell type is shown as *n*. For each recording, the centre of the receptive field and the acceptance angles were determined at the moment in time, in the spatiotemporal impulse response, at which the response amplitude was maximal. Where possible, centre points and acceptance angles are shown as mean ± standard deviation. Values given for the tri-ocellar neuron MB describe only the region of receptive field falling within the field of view of the lateral ocellus. The medial receptive field of this neuron has been described previously (Berry et al. 2006). All values are underestimated (>) for LI₂, as much of the receptive field of this neuron lay outside the limits of the stimulus. Values used to determine centre point values are absolute values, such that the results given indicate the centre of receptive fields for neurons in one lateral ocellus. As the two lateral ocelli are symmetrical, L-neurons in the opposite lateral ocellus have receptive fields of the same size and location, but of opposite sign in azimuth. The point (0, 0) lies at the optical axis of the median ocellus with positive-going elevation values representing the upward direction

decreasing resolution and sensitivity towards the periphery, and that a value of 30% tapetal sheathing minimises the detrimental effects of optical cross-talk, and maximises the available resolution for the central most rhabdoms in the retina (Berry et al. 2007a). As the anatomical arrangement of the dorsal retina of the lateral ocellus directly resembles the anatomical arrangement of the median ocellar retina in the vertical plane, it may be expected that the two share similar principles of design. The dorsal retina therefore appears to extend the predictions from the median ocellus (Stange et al. 2002; Berry et al. 2006), namely it is specifically adapted to resolve horizontally extended features of the world, across a narrow band of elevational space.

Conversely, the ventral retina is directed skyward and receives a poorly focussed image from the lens. Tapetally sheathed rhabdom bases are located well distal to the focal plane of the lens, and therefore spatial information processing is unlikely to be of high importance in the ventral retina.

Anatomy and classification of dragonfly L-neurons

The morphology of dragonfly lateral ocellar L-neurons has been previously investigated by Chappell et al. (1978). In this study, cobalt fills of the ligated ocellar nerves of *Aeschna tuberculifera* and *Anax junius* revealed the presence of four large diameter neurons. Two of these neurons crossed the midline of the brain to terminate in the contralateral posterior slope, while the remaining two neurons terminated in the ipsilateral posterior slope.

In *Hemicordulia*, the iontophoretic injection of dye into individual neurons also gives evidence for the

presence of four L-neurons in the lateral ocelli. In contrast, however, evidence for the existence of contralateral L-neurons was not found. Rather, the L-neurons described here (with the exception of MB) either projected to the ipsilateral posterior slope, or descended to the suboesophageal ganglion (Fig. 7). This is supported by receptive field recordings, which were obtained from many more L-neurons than could be successfully identified by iontophoretic dye injection. In no case was a receptive field obtained that could not be attributed to one of the four L-neurons described above. This leads us to suggest that the four neurons described here constitute the entire set of L-neurons innervating the lateral ocelli of *Hemicordulia*, and that additional neurons do not exist. As contralateral neurons have thus far been described only for species of the Aeschnidae family, there is a possibility that these fibres are specific to this family, and absent in Corduliidae.

Descending L-neurons of the dragonfly ocelli

A previously undescribed descending neuron, termed LD, is described above. This neuron bears many similarities to the MD neurons of the median ocellus (Berry et al. 2006), and it appears that these neurons form a specific descending sub-class of L-neuron.

Descending neurons are the only L-neurons known to produce regenerative action potentials. The situation is similar in bees, where Milde and Homberg (1984) describe L_D neurons (L-neurons descending into the ventral nerve cord) as always producing spikes. Berry et al. (2006) suggested that the presence of regenerative potentials in MD may be related to the longer transmission length of these neurons, and this

suggestion appears to be supported here by the long transmission length of LD.

In addition, Milde and Homberg (1984) find that only descending neurons may carry information from sensory systems other than the ocelli. The MD neurons support this hypothesis, where wind and wing movements affect the firing frequency of these neurons. Multimodal transmission can also be observed in LD, where gently blowing an air stream funnelled through a pipette around the head of a dragonfly can result in an inhibition of firing frequency (unpublished observation). The insect deutocerebrum is generally considered to be an olfactory processing area, but also contains an antennal mechanosensory and motor centre (AMMC), with some neurons in this area responding to puffs of air (reviewed in Homberg et al. 1989). Thus, the deutocerebral terminations of LD and MD are the most likely site of sensory integration with head mechanoreceptors, although the deutocerebrum of dragonflies is notably poorly developed (Schachtner et al. 2005). The effect of wing motion on L-neuron physiology was not tested here, but was extensively tested by Kondo (1978), who analysed extracellular suction electrode recordings of the dragonfly lateral ocellar nerve. Kondo (1978) found that forced or self-invoked wing movements, or electrical stimulation of wing sensory organs, evoked bursting discharges in a large efferent unit in the lateral ocellar nerve. These discharges disappeared when the suboesophageal connectives were severed. This large fibre also received input from the compound eyes, the illumination of which resulted in increased firing frequency when all ocellar nerves were ligated (when the ocellar nerves are intact, the light inhibitory response of the ocelli appears to override the light excitatory response of the compound eyes). Kondo (1978) considered this large fibre as solely efferent, and independent of a large afferent fibre, which showed a reduction in firing frequency upon illumination of the lateral ocellus. Given that it is now known that multiple modalities can be conducted in single ocellar L-neurons, it appears that both the large afferent and the large efferent fibre may be one and the same neuron, namely LD. The function of multimodal input in descending ocellar neurons remains puzzling. Their exceptionally large diameter, and more direct connection to motor control systems suggests that rapid conduction velocity is even more important in descending L-neurons than in other L-neurons.

Preservation of spatial information

Evidence for the preservation of spatial information at the level of the second-order neurons of the dragonfly

median ocellus was given in a previous study (Berry et al. 2006). The work described here extends this finding to second-order neurons of the lateral ocelli of the same animal.

The receptive fields of LI₁ and LD follow the pattern described for the L-neurons of the median ocellus, namely the receptive fields of these neurons are equatorially centred and elliptical, being much narrower in elevation than in azimuth. Indeed mean acceptance angles of 13.3° and 12.0°, respectively, are less than the elevational acceptance angles of photoreceptors in the median ocellus, which van Kleef et al. (2005) found to be 15°. The results suggest that LI₁ and LD receive the majority of their input from the dorsal retina, which possesses an optical fovea for high resolution along the equatorial plane. The receptive field of LI₂, on the other hand, is elevationally extended and centred well above the equator, in a slightly backward direction. Thus this L-neuron presumably receives the majority of its input from the ventral retina.

The axonal terminations of neurons terminating in the PSL also match the general trend observed in the median ocellus: L-neurons with more lateral fields of view terminate in more lateral regions of the PSL (Chappell et al. 1978; Patterson and Chappell 1980). There is the possibility that spatial mapping onto third-order descending interneurons originating from the PSL exists, inviting verification by receptive field determination of descending interneurons with ocellar input.

Functional roles of the dragonfly ocellar system

Previous determination of the receptive fields of median ocellar L-neurons yielded the conclusion that this system forms a one-dimensional representation of the equator (Berry et al. 2006). Combining the previous results with the findings described here from lateral ocellar L-neurons supports and extends this conclusion (Fig. 10). The ocellar L-neurons constitute an assembly of seventeen sensors that (with the exception of LI₂) together resolve some spatial detail of the equator over a wide azimuthal area. In level flight, the equatorial plane is aligned with the horizon, which indicates that the system is designed to be maximally sensitive over a narrow strip along the horizon. Sampling density is highest near the centre of the median ocellus, where some points of visual space are sampled by as many as six L-neurons.

Multiple sampling stations across an extended azimuthal space may impart a number of benefits to an attitude stabilising system. These benefits include; error suppression or signal averaging, yaw detection and

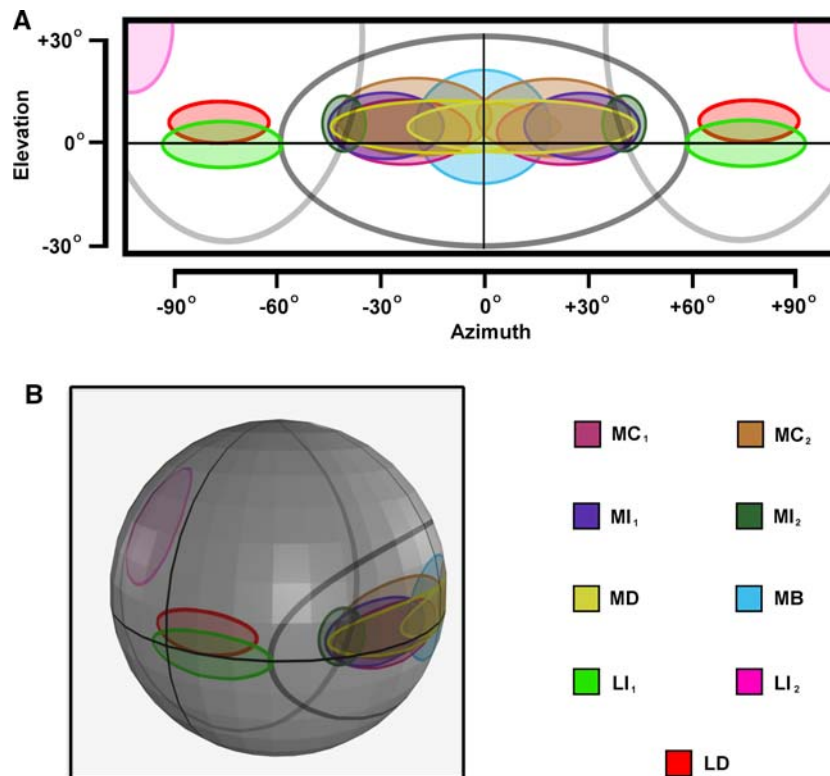


Fig. 10 Schematic illustration of the receptive fields of known L-neurons of the median and lateral ocelli. Receptive fields have been projected onto a plane in **a**, and wrapped onto a sphere in **b**. In the case of **a**, the *outer black box* represents the limits of the stimulus used to obtain receptive fields. Receptive fields are simplified to ellipses, with values for the major and minor axes defined by mean horizontal and vertical acceptance angles. The origins of the ellipses are defined as the mean receptive field centre points of each neuron. In the case of median ocellar L-neurons, values were taken from Berry et al. (2006). In the case of lateral ocellar L-neurons, values are given in Table 2. Fields of

view of the median (*dark grey ellipse*) and lateral (*light grey ellipse*) ocelli were determined from the angular range over which tapetal reflections are visible from the eyes (Stange et al. 2002). Centre points and acceptance angles of both MI₂ and LI₂ are underestimated, as the receptive fields of these neurons exceeded the limits of the stimulus. In the case of LI₂ the recorded acceptance angles have been doubled in **b**, as the centre point of this neuron lay outside the limits of the stimulus in both elevation and azimuth. The point (0,0) lies at the optical axis of the median ocellus, which is approximately equivalent to the long body axis of a dragonfly in level flight

object avoidance (Berry et al. 2006). Alternatively, if the system is capable of some resolution, especially in the vertical plane, the line of demarcation between the ground and the sky may be used as an absolute reference point from which to correct body attitude.

Comparison of intensity levels alone, as is generally considered to be the function of the ocelli in pterygote insects, can result in substantial correction errors when one ocellus is strongly illuminated by some feature of the external world, for example, the sun (Chahl et al. 2003). Additionally, changes in yaw are not distinguishable by such a system. Indeed, when the sun is not directly overhead, changes in yaw may be incorrectly perceived as a change in roll or pitch if one of the three ocelli is directed towards the sun during the yaw rotation.

These errors may be avoided if the horizon itself is used to define and correct body attitude during flight.

A horizon localizing system requires the ability to resolve at least two points spatially separated in the vertical plane (one for the “sky” and one for the “ground”), and strongly benefits from the ability to follow movements of the edge between these two stations. Some evidence of this capability has been given by the observation of directionally selective responses from the ventral nerve cord of the dragonfly. Zenkin and Pigarev (1971) found both median and lateral ocellus driven units in the ventral nerve cord which responded to the upward and downward motion of gratings in a directionally selective manner. These responses could be attributed to stimulation of the ocelli alone, as they were abolished upon occlusion of the ocelli, but not the compound eyes.

Earlier work suggested that the median ocellus may be specifically adapted to detect and track movements of the horizon for the purpose of correcting deviations

around the pitch axis (Stange et al. 2002; Berry et al. 2006). The finding here that the dorsal retina of the lateral ocelli also appears to be adapted for resolving horizontally extended features of the world suggests that this retina may subservise a similar function. In this case, the LI₁ and LD neurons, being centred close to the equator and at azimuths of nearly 90°, would be ideally suited for the fine correction of roll, given that the largest movement vectors during deviations around the roll axis occur at this location (Neumann and Bülthoff 2002). This is essentially the opposite of the single sensor hypothesis, where the ocelli act as ‘rough and ready’ detectors of body attitude (Wilson 1978).

Note, however, that the one-dimensional mapping arrangement of ocellar L-neurons makes them most effective for fine attitude control when the dragonfly is already centred close to a level attitude, for example, during hover. The narrow elevational fields of these neurons limit the range over which attitude may be encoded: large deviations around the pitch or roll axes render the horizon out of the field of view of the majority of L-neurons. Interestingly, however, a halfring of equatorial sensors that extends over 180° in azimuth will always be bisected by the horizon at least once, irrespective of body attitude. Such a system is theoretically capable of determining body attitude at any orientation, either by determining the location and angle of intersection with the horizon, or by luminance cues.

Additionally, if the horizon falls out of the field of view of an L-neuron it is possible that it then functions as a small-field illumination detector. Small deviations from a level attitude are more readily apparent to correctly positioned small-field sensors than to wide-field sensors, as the encoded intensity is more strongly shifted towards a mean ambient value in the latter.

In this respect, the field of view and underfocussed nature of the ventral retina is particularly interesting. With regard to attitude stabilization, lack of resolving power in the ventral retina is not surprising, given that the area of visual space above the equatorial plane is largely devoid of spatial features. Therefore, little is to be gained from spatially mapping this region (Wehner 1981; Neumann and Bülthoff 2002). On the other hand, luminance cues obtained from this region of visual space may contain valuable information about roll attitude, especially during large deviations around the roll axis.

Experienced human pilots know that if an aircraft has assumed an extreme attitude, the first thing that must be done to achieve stable flight is to correct alignment around the roll axis (M. Garratt, personal communication). In certain conditions, an attempt to

correct pitch first may actually exacerbate the problem. As the receptive fields of LI₂ are centred at least 33° above the equator, the largest intensity differences between this neuron pair would be encoded during a very sharply banked turn. In a simplified world, and assuming the receptive field of LI₂ extends approximately 40° in elevation, a roll angle of 73° would be required to give maximum intensity differences between the pair of LI₂ neurons (such that one neuron views ground and the other sky). This pair of neurons may therefore act as emergency roll correctors.

Acknowledgments This work was sponsored by the Air Force Office of Scientific Research (AFOSR), contract AOARD-03-4009. We thank Dr. Michael Ibbotson for providing some of the necessary software to generate three-dimensional reconstructions. The experiments described herein comply with guidelines supplied by the Animal Experimentation Ethics Committee of the Australian National University, and also with the current laws of Australia, where the experiments were performed.

References

- Berry R, Stange G, Olberg R, van Kleef J (2006) The mapping of visual space by identified large second-order neurons in the dragonfly median ocellus. *J Comp Physiol A* 192:1105–1123
- Berry RP, Stange G, Warrant EJ (2007a) Form vision in the insect dorsal ocelli: an anatomical and optical analysis of the dragonfly median ocellus. *Vis Res* (in press)
- Berry RP, Warrant EJ, Stange G (2007b) Form vision in the insect dorsal ocelli: an anatomical and optical analysis of the locust ocelli. *Vis Res* (in press)
- Campbell FW, Green DG (1965) Optical and retinal factors affecting visual resolution. *J Physiol* 181:576–593
- Campbell FW, Gubisch RW (1966) Optical quality of the human eye. *J Physiol* 186:558–578
- Chahl J, Thakoor S, Le Bouffant N, Stange G, Srinivasan MV, Hine B, Zornetzer S (2003) Bioinspired engineering of exploration systems: a horizon sensor/attitude reference system based on the dragonfly ocelli for Mars exploration applications. *J Robotic Syst* 20(1):35–42
- Chappell RL, Dowling JE (1972) Neural organization of the median ocellus of the dragonfly. I. Intracellular electrical activity. *J Gen Physiol* 60:121–147
- Chappell RL, Goodman LJ, Kirkham JB (1978) Lateral ocellar nerve projections in the dragonfly brain. *Cell Tissue Res* 190:99–114
- Cornwell PB (1955) The functions of the ocelli of *Calliphora* (Diptera) and *Locusta* (Orthoptera). *J Exp Biol* 32:217–237
- Goodman LJ (1981) Organisation and physiology of the insect dorsal ocellar system. In: Autrum H (eds) *Handbook of sensory physiology*, Vol VII 6C. Springer, Berlin, pp 201–286
- Homann H (1924) Zum Problem der Ocellenfunktion bei den Insekten. *Z Vergl Physiol* 1:541–578
- Homberg U, Christensen TA, Hildebrand JG (1989) Structure and function of the deutocerebrum in insects. *Annu Rev Entomol* 34:477–501
- James AC, Ruseckaite R, Maddess T (2005) Effect of temporal sparseness and dichoptic presentation on multifocal visual evoked potentials. *Vis Neur* 22:45–54

- Kondo H (1978) Efferent system of the lateral ocellus in the dragonfly: Its relationships with the ocellar afferent units, the compound eyes, and the wing sensory system. *J Comp Physiol A* 125:341–349
- Labhart T, Nilsson D-E (1995) The dorsal eye of the dragonfly *Sympetrum*: specializations for prey detection against the blue sky. *J Comp Physiol A* 176:437–453
- Land MF (1981) Optics and vision in invertebrates. In: Autrum H (ed) *Handbook of sensory physiology*, Vol VII 6B. Springer, Berlin, pp 471–592
- Milde J, Homberg U (1984) Ocellar interneurons in the honeybee: characteristics of spiking L-neurons. *J Comp Physiol A* 155:151–160
- Mizunami M (1994). Functional diversity of neural organization in insect ocellar systems. *Vision Res* 35:443–452
- Mobbs PG, Guy RG, Goodman LJ, Chappell RL (1981) Relative spectral sensitivity and reverse Purkinje shift in identified L-neurons of the ocellar retina. *J Comp Physiol A* 144:91–97
- Neumann TR, Bülthoff HH (2002) Behaviour-oriented vision for biomimetic flight control. In: *Proceedings of the EPSRC/BBSRS international workshop on biologically inspired robotics* 14–16, pp 196–203
- Parry DA (1947) The function of the insect ocellus. *J Exp Biol* 24:211–219
- Parsons MM, Krapp HG, Laughlin SB (2006) A motion-sensitive neurone responds to signals from the two visual systems of the blowfly, the compound eyes and ocelli. *J Exp Biol* 209:4464–4474
- Patterson JA, Chappell RL (1980) Intracellular responses of procion filled cells and whole nerve cobalt impregnation in the dragonfly median ocellus. *J Comp Physiol A* 139:25–39
- Rosser BL (1974) A study of the afferent pathways of the dragonfly lateral ocellus from extracellularly recorded spike discharges. *J Exp Biol* 60:135–160
- Ruck P (1958) A comparison of the electrical responses of compound eyes and dorsal ocelli in four insect species. *J Insect Physiol* 2:261–274
- Ruck P (1961a) Electrophysiology of the insect dorsal ocellus. I. Origin of the components of the electroretinogram. *J Gen Physiol* 44:605–627
- Ruck P (1961b) Electrophysiology of the insect dorsal ocellus. II. Mechanism of generation and inhibition of impulses in the ocellar nerve of dragonflies. *J Gen Physiol* 44:629–639
- Ruck P, Edwards GA (1964) The structure of the insect dorsal ocellus. I. General organization of the ocellus in dragonflies. *J Morphol* 115:1–26
- Schachtner J, Schmidt M, Homberg U (2005) Organization and evolutionary trends of primary olfactory brain centers in Tetraconata (Crustacea + Hexapoda). *Arthropod Struct Dev* 34:257–299
- Schuppe H, Hengstenberg R (1993) Optical properties of the ocelli of *Calliphora erythrocephala* and their role in the dorsal light response. *J Comp Physiol A* 173:143–149
- Simmons PJ (1982a) The operation of connexions between photoreceptors and large second-order neurons in dragonfly ocelli. *J Comp Physiol* 149:389–398
- Simmons PJ (1982b) Transmission mediated with and without spikes at connexions between large second-order neurones of locust ocelli. *J Comp Physiol A* 147:401–414
- Stange G, Howard J (1979) An ocellar dorsal light response in a dragonfly. *J Exp Biol* 83:351–355
- Stange G (1981) The ocellar component of flight equilibrium control in dragonflies. *J Comp Physiol A* 141:335–347
- Stange G, Stowe S, Chahl JS, Massaro A (2002) Anisotropic imaging in the dragonfly median ocellus: a matched filter for horizon detection. *J Comp Physiol A* 188:455–467
- Taylor CP (1981) Contribution of compound eyes and ocelli to steering of locusts in flight. I. Behavioural analysis. *J Exp Biol* 93:1–18
- van Kleef J, James AC, Stange G (2005) A spatiotemporal white noise analysis of photoreceptor responses to UV and green light in the dragonfly median ocellus. *J Gen Physiol* 126:481–497
- Warrant EJ, Kelber A, Wallén R, Weislo WT (2006) Ocellar optics in nocturnal and diurnal bees and wasps. *Arthropod Struct Dev* (in press)
- Warrant EJ, McIntyre PD (1993) Arthropod eye design and the physical limits to spatial resolving power. *Prog Neurobiol* 40:413–461
- Warrant EJ, Nilsson D-E (1998) Absorption of white light in photoreceptors. *Vision Res* 38(2):195–207
- Weber G, Renner M (1976) The ocellus of the cockroach *Periplanta americana* (Blattariae). Receptor area. *Cell Tissue Res* 168:209–222
- Wehner R (1981) Spatial vision in arthropods. In: Autrum H (ed) *Handbook of sensory physiology*, Vol VII 6C. Springer, Berlin, pp 287–616
- Wilson M (1978) The functional organisation of locust ocelli. *J Comp Physiol A* 124:297–316
- Zenkin GM, Pigarev IN (1971) Optically determined activity in the cervical nerve chain of the dragonfly. *Biofizika* 16:299–306